J. of Supercritical Fluids 76 (2013) 41–47

Contents lists available at SciVerse ScienceDirect

The Journal of Supercritical Fluids

journal homepage: www.elsevier.com/locate/supflu

# Kinetic model for isopropanol oxidation in supercritical water in hydrothermal flame regime and analysis

J.P.S. Queiroz, M.D. Bermejo*, M.J. Cocero

*High Pressure Process Group, Department of Chemical Engineering and Environmental Technology, University of Valladolid, Doctor Mergelina, s/n, 47011 Valladolid, Spain*

ARTICLE INFO

*Article history:*
Received 27 November 2012
Received in revised form 23 January 2013
Accepted 24 January 2013

*Keywords:*
Kinetics
Parameter identification
Hydrothermal flames
CFD modeling
Supercritical water oxidation
Mathematical modeling

ABSTRACT

Supercritical water oxidation (SCWO) in hydrothermal flame regime has advantages over the oxidation in flameless regime. The main advantage is that the feed can be injected into the reactor at low temperatures, avoiding plugging and corrosion problems in a preheating system. However, there is a lack of kinetic data capable of properly describing the flame regime oxidation. In this study, new global reaction rate parameters for the oxidation of isopropyl alcohol in hydrothermal regime were adjusted from temperature profiles of our group's previous experimental data. The kinetics obey first order rate with regard to the fuel and the oxidant, and follows the Arrhenius law. The parameters are $k_0 = (9.308 \pm 3.989) \times 10^7$ ($m^3\ s^{-1}\ kmol^{-1}$) and $E_a = 89.441 \pm 2.457$ ($kJ\ mol^{-1}$), and the least square error of the fitting was 10.8%. This kinetic model was applied in a parametric analysis of flame formation, and it was used to analyze the behavior of a supercritical water oxidation vessel reactors. The kinetic model is able to describe the behavior of the vessel reactor when working in steady state hydrothermal flame regime at subcritical injection temperatures (246 °C). The model predicts both flameless and hydrothermal flame regimes.



## 1. Introduction

Supercritical water oxidation (SCWO) in hydrothermal flame regime is a promising technology for the total destruction of waste because overcomes the challenges that have delayed the successful and profitable commercialization of this technology: corrosion, salt deposition and high energy demand [1,2]. Working with residence times below 1 s, the process can be performed in microreactors. When the temperature of the mixture becomes greater than the ignition temperature a flame is produced, and in this kind of dense aqueous environment it is known as hydrothermal flame [3]. Hydrothermal flames were referred to for first time by Franck and coworkers [4]. Several research groups have developed reactors working with a hydrothermal flame as heat source [5,6], since SCWO reactors using a hydrothermal flame have a number of advantages [3]:

- Pollutants can be destroyed in residence times of a few milliseconds.
- The higher operation temperatures improve energy recovery.
- It is possible to initiate the reaction with feed injection temperatures near to room temperature [7].

This last point presumes an advantage from the operational and energetic integration points of view, as it avoids problems of plugging and corrosion in a preheating system.

The High Pressure Process Group (HPPG) of the University of Valladolid (UVa) (Spain) recently demonstrated the formation of hydrothermal flames in tubular reactors [8]. Using this simple device, the extinction temperatures of the flame could not be reduced to less than 370 °C. Vessel reactors have shown to be more successful in maintaining steady stable hydrothermal flames with injection temperatures near to room temperature [5,6,9]. The flame stability is related to the injection temperature and flow velocity, and vessel reactors provide flow velocities that are compatible with hydrothermal flame front velocities [10]. It is thought that vessel reactors provide a space for recirculation in which the cold reagents are preheated to the ignition temperature and are brought into contact with the radicals already formed, making it possible for the flame to be formed. CFD simulations of these reactors show the existence of a flame front where most of the reaction takes place [11].

This development on the SCWO process has been possible, in part, as a result of the increase in the quantitative understanding of the SCWO reaction initiation rates of different types of organic species at the lower temperatures of 450–500 °C [12]. The focus of

* Corresponding author. Tel.: +34 983423166.
*E-mail addresses:* joao.deq@gmail.com (J.P.S. Queiroz), mdbermejo@iq.uva.es, mdbermejo@gmail.com (M.D. Bermejo), mjcocero@iq.uva.es (M.J. Cocero).

0896-8446/$ – see front matter © 2013 Elsevier B.V. All rights reserved.
http://dx.doi.org/10.1016/j.supflu.2013.01.021

**Nomenclature**

| | |
|---|---|
| $C$ | molar concentration (kmol m$^{-3}$) |
| $E_a$ | activation energy (kJ mol$^{-1}$) |
| $\Delta H_r$ | heat of reaction (J kmol$^{-1}$) |
| $M$ | molecular weight (kg kmol$^{-1}$) |
| $R$ | universal gas constant (J mol$^{-1}$ K$^{-1}$) |
| $R_k$ | species source (kmol m$^{-3}$ s$^{-1}$) |
| $S$ | cross section (m$^2$) |
| $S_h$ | energy source (J m$^{-3}$ s$^{-1}$) |
| $T$ | temperature (K) |
| $V$ | molar volume (m$^3$ mol$^{-1}$) |
| $X$ | auxiliary parameter |
| $c_p$ | constant pressure heat capacity (J kg$^{-1}$ K$^{-1}$) |
| $f_{obj}$ | objective function |
| $h$ | specific enthalpy (J kg$^{-1}$) |
| $k_0$ | Arrhenius pre-exponential factor (s m$^3$ kmol$^{-1}$) |
| $\dot{m}$ | mass flow (kg s$^{-1}$) |
| $r$ | reaction rate (kmol m$^{-3}$ s$^{-1}$) |
| $t$ | time (s) |
| $u$ | velocity (m s$^{-1}$) |
| $vt$ | translated volume (cm$^3$ mol$^{-1}$) |
| $w$ | mass fraction |
| $y^+$ | dimensionless wall distance |
| $z$ | longitudinal coordinate (m) |

*Greek symbols*

| | |
|---|---|
| $\lambda$ | thermal conductivity (W m$^{-1}$ K$^{-1}$) |
| $\rho$ | density (kg m$^{-3}$) |
| $\tau$ | stress tensor (N m$^{-2}$) |

*Subscripts*

| | |
|---|---|
| $i, j, l$ | directions |
| $k$ | species |
| $t$ | turbulent |

*Abbreviations*

| | |
|---|---|
| CFD | computational fluid dynamics |
| CI | confidence interval |
| PR | Peng–Robinson equation of state |
| IPA | isopropyl-alcohol |
| SCW | supercritical water |
| SCWO | supercritical water oxidation |
| TOC | total organic carbon |
| TWR | transpiring wall reactor |
| VTPR | volume translated Peng–Robinson equation of state |

these kinetic studies has typically been on model compounds rather than on actual waste. These compounds have been chosen because they contain key functional groups of importance and/or represent the rate limiting step in the breakdown of a range of complex waste species. Considering only homogeneous reactions without catalysts, extensive data on SCWO kinetics have been reported for a number of model compounds [12–16]. However, these kinetic data from literature are not able to describe flame regime oxidation [8]. Concentration profiles in the SCWO reactor are very difficult to obtain due to fast reaction rates and usually only global conversions are reported, except when optical devices are used [17–19]. The lack of kinetic models is one of the reasons why most of the modeling of hydrothermal flames is based on mixing controlled reactions [11,20]. This approach is valid for non-premixed flames at high temperatures since it assumes that chemical reaction is fast compared to the transport processes in the flow. The characteristics of our system are similar to premixed flames, where fuel and oxidant are totally mixed and chemical reaction is important.

In this work, a new kinetic model for the supercritical water oxidation of isopropyl alcohol in flame regime has been adjusted using our group's previous experimental data [8]. Temperature profiles were used to fit kinetic parameters, by developing a mathematical model. This model is able to reproduce experimental data using either air or oxygen as the oxidant. A parametric analysis showed that the model is in accordance with the work of Serikawa [21]. The adjusted kinetic model has been used to make an analysis of the behavior of a vessel reactor, in particular of the transpiring wall reactor with an internal hydrothermal flame studied at the University of Valladolid.

## 2. Experiments

Experimental data used for adjusting the kinetic parameters of the oxidation of isopropyl-alcohol at hydrothermal flame regime were performed at the University of Valladolid's SCWO pilot plant, which had been adapted to work with tubular mixers as described by Bermejo et al. [8]. The pilot plant has a maximum treatment capacity of 20 kg/h feed and uses air as an oxidant compressed by a four staged reciprocating compressor. Both, air and feed are electrically preheated before being introduced into the tubular reactor, which consists of a commercial Ni-alloy tube of 1/4″ diameter and 1.5 m length. The reaction was monitored by measuring temperatures at the mixing point and at several points inside the reactor, and also by determining the total organic carbon (TOC) of the effluent. After leaving the reactor the reaction mixture is quenched. The products are cooled down to room temperature in the intercoolers, and after depressurization, samples of the liquid and gas effluents can be taken.

Additional experiments using pure $O_2$ as the oxidant were performed in a similar tubular reactor, installed in a demonstration plant of the University of Valladolid situated in the premises of the CETRANSA company in Santovenia de Pisuerga (Valladolid). In this case, cryogenic $O_2$ was pumped until reaching operational pressure and brought to room temperature by an evaporator. The reactor was a Ni-alloy tube of 1/4″ diameter and 2 m length. The demonstration plant is already described in previous work [22].

To determine the kinetic parameters, data from 24 experiments using air and 8 using $O_2$, under different inlet conditions were used.

Once the kinetic model was obtained, it was introduced in a previous model of the transpiring wall reactor working at the same University of Valladolid pilot plant as described by Bermejo et al. [23], and the results of simulations were compared to experimental data. The transpiring wall reactor consists of a stainless steel pressure shell with a volume of 10 L. It contains a reaction chamber surrounded by a porous wall through which clean water circulates. The feed and the air are introduced into the reactor through its lower part, and they are fed through the injector into the upper part of the reaction chamber; the reagents flow downwards mixing with the clean water that enters the reactor through the transpiring wall, and decontaminated water leaves the reactor through its lower part. More constructive details of the reactor can be found elsewhere [10,23]. In order to follow the reaction, the temperature is measured at several points in the reaction chamber.

## 3. Modeling

### 3.1. Tubular reactor

A simple model of the tubular reactor described in Section 2 was programmed in order to fit the kinetic parameters of IPA oxidation, by minimizing the difference between experimental and calculated

**Table 1**
Volume translation at 23 MPa for application in VTPR-EoS.

| | $vt$ (cm$^3$ mol$^{-1}$) |
|---|---|
| $H_2O$ | 4.291073 |
| $O_2$ | −2.545861 |
| $N_2$ | −3.743775 |
| $CO_2$ | 1.284445 |
| IPA | 3.721115 |

temperatures at several points inside the reactor. The following assumptions were made:

1. Plug flow is assumed and the feed and oxidant streams are presumed to be completely mixed at the reactor inlet. There is neither axial nor radial dispersion. This hypothesis of complete mixing was verified by CFD simulation (Section 4.1).
2. The model assumes that the oxidation of the isopropyl-alcohol (IPA) takes place in a single step, leading to the formation of carbon dioxide and water as shown in Eq. (1).

$$C_3H_8O + 4.5O_2 \rightarrow 3CO_2 + 4H_2O \quad (1)$$

3. The pressure remains constant at 23 MPa along the reactor.
4. Enthalpy of the mixture is given by the original Peng–Robinson Equation of State (PR-EoS) [24]. Densities are calculated by the PR-EoS with constant volume translation (VTPR-EoS) [25]. In both cases van der Waals mixing rules are used. The volume correction was adjusted for each pure component using density data from the NIST database [26] and from Aspen Plus calculations using the SR-Polar-EoS [27] at operating pressure, similar to the procedure used by Lieball [28]. Table 1 presents the volume correction for the five substances that compose the system. Additional information about the volume correction calculation can be found in Appendix A. The translated volume of the mixture is a linear function of the component mole fractions.

For a differential control volume inside a plug flow reactor, the material balance for the fuel (IPA) results in Eq. (2):

$$\frac{dw_{IPA}}{dz} = -\frac{r \cdot M_{IPA} \cdot S}{\dot{m}} \quad (2)$$

where $w_{IPA}$ is mass fraction of isopropyl-alcohol, $z$ the length of the tubular reactor, $r$ the reaction rate, $M_{IPA}$ the molecular weight of isopropyl-alcohol, $S$ the cross section of the tubular reactor, and $\dot{m}$ the total mass flow.

The energy balance for the same control volume leads to Eq. (3).

$$\frac{dh}{dz} = \frac{\Delta H_r \cdot r \cdot S}{\dot{m}} \quad (3)$$

where $h$ is the specific enthalpy, and $\Delta H_r$ is the heat of reaction, calculated from the enthalpies of formation of each component. Assuming no pressure changes $dh = c_p dT$, Eq. (3) can be rewritten as Eq. (4).

$$\frac{dT}{dz} = \frac{\Delta H_r \cdot r \cdot S}{\dot{m} \cdot c_p} \quad (4)$$

where $c_p$ is the specific heat capacity of the mixture. In Eqs. (2)–(4) the reaction rate $r$ can be described according to the Arrhenius law:

$$r = k_0 \exp\left(-\frac{E_a}{RT}\right) C_{IPA} C_{O_2} \quad (5)$$

Reaction order regarding IPA is assumed as equal to 1, as suggested in previous works [29,12]. Oxygen reaction order cannot be assumed as 0, since there is no significant excess in experimental data. Therefore, the model assumes first order reaction behavior for both fuel and oxidant. The assumed order of reaction gives the S-shape profiles of temperature observed in experimental data.

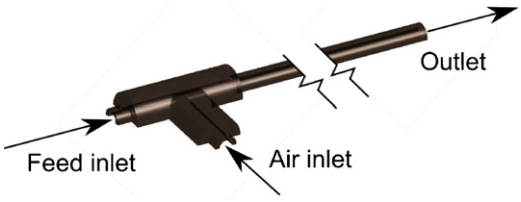


**Fig. 1.** 3D tee-junction geometry model used in CFD simulation.

In order to improve the optimization process, two auxiliary variables have been defined: $X_1 = \ln(k_0)$ and $X_2 = E_a/(R \cdot 850)$. Also, for convenience, concentrations were substituted by mass fraction. Thus, Eq. (5) can be rewritten:

$$r = \exp\left(X_1 - \frac{X_2 \cdot 850}{T}\right) \frac{w_{ipa}}{M_{ipa}} \frac{w_{O_2}}{M_{O_2}} \rho^2 \quad (6)$$

where $\rho$ is the density of the mixture. The value 850 is a characteristic temperature and was taken in order to give $X_1$ and $X_2$ the same order of magnitude.

The optimization procedure uses the Matlab function `lsqnonlin`, which consists of a non-linear least-square solver with Levenberg–Marquardt algorithm [30,31]. The function to be minimized is:

$$f_{obj} = \sum_{k=1}^{n} (T_k - \widehat{T}_k)^2 \quad (7)$$

where $T_k$ are experimental temperatures and $\widehat{T}_k$ the calculated temperatures. These temperatures are obtained by solving the set of equations for $w_{IPA}$ (Eq. (2)) and $T$ (Eq. (4)) simultaneously using Matlab solver `ode15s`. The parameters fitted are $X_1$ and $X_2$ from which the Arrhenius parameters can be obtained.

### 3.2. Study of the mixing process of water and air flow

The assumption of instantaneous mixing taking place in the tubular reactor was verified by 3D simulation of the tee-junction. The extent to which air and feed flow are totally mixed was investigated by obtaining the concentration profiles in different lengths of the reactor. In these simulations a non-reacting flow was considered. The geometry of the model includes the tee-junction and a 25 cm segment of the reactor and the metallic wall, as shown in Fig. 1. The domain is limited by the longitudinal plane of symmetry and half of the tee and tube wall. The mesh is composed of 436,000 mixed cells at the fluid region, and 529,000 tetrahedral cells at the solid region. The fluid region mesh is formed by hexahedral cells at the near wall region and tetrahedral cells at core region, assuring an $y^+$ value below 5.

The model includes the five species that constitute the system: water, oxygen, nitrogen, carbon dioxide and isopropyl-alcohol, and solves the Reynolds-averaged transport equations [33] for mass, momentum, energy and species, as shown in Eqs. (8)–(11):

$$\frac{\partial \rho}{\partial t} + \frac{\partial}{\partial x_i}(\rho u_i) = 0 \quad (8)$$

$$\frac{\partial}{\partial t}(\rho u_i) + \frac{\partial}{\partial x_j}(\rho u_i u_j) = -\frac{\partial p}{\partial x_i} + \frac{\partial}{\partial x_j}(\tau_{ij} - \rho \overline{u_i' u_j'}) \quad (9)$$

$$\frac{\partial}{\partial t}(\rho E) + \frac{\partial}{\partial x_i}[u_i(\rho E + p)] = \frac{\partial}{\partial x_j}\left((\lambda + \lambda_t)\frac{\partial T}{\partial x_j}\right) + S_h \quad (10)$$

$$\frac{\partial}{\partial t}(\rho w_k) + \frac{\partial}{\partial x_i}(\rho u_i w_k) = -\frac{\partial}{\partial x_i}\left[\rho(D + D_t)\frac{\partial w_k}{\partial x_i}\right] + R_k \quad (11)$$

where $u_i$ is the fluid velocity in the $x_i$ direction, $p$ the pressure, $E$ is the total energy and $w_k$ the mass fraction of species $k$. The source terms $S_h$ and $R_k$ represent the heat of reaction and the net rate of species $k$ production by chemical reaction. Thus, for the non-reacting flow model, their values are zero. The viscous stress tensor $\tau_{ij}$ is shown in Eq. (12):

$$\tau_{ij} = \mu\left(\frac{\partial u_i}{\partial x_j} + \frac{\partial u_j}{\partial x_i} - \frac{2}{3}\delta_{ij}\frac{\partial u_l}{\partial x_l}\right) \tag{12}$$

where $\mu$ is the molecular viscosity calculated as a mass-fraction average of the properties of the pure components.

In Eq. (10), the total energy $E$ is:

$$E = h - \frac{p}{\rho} + \frac{u^2}{2} \tag{13}$$

In Eqs. (8)–(13) $\rho$ is the mixture density calculated by VTPR-EoS, $\lambda$ the thermal conductivity calculated by TRAPP method for high pressure fluids [33], $D$ the diffusion coefficient calculated as the mass-fraction average of the pure species, and specific enthalpy $h$ is given by PR-EoS. The turbulent thermal conductivity $\lambda_t$, the turbulent diffusion coefficient $D_t$ and the Reynolds stress tensor $-\rho\overline{u_i'u_j'}$ are defined according to the turbulence model being used. In this work, the Realizable $k$–$\epsilon$ model has been used in order to model turbulence, as suggested by Sierra-Pallares et al. [34], with enhanced wall treatment.

The model was solved using the commercial CFD software ANSYS FLUENT 12.0, with segregated pressure based solver, SIMPLE algorithm for pressure–velocity coupling, and second order upwind discretization for energy, momentum, $k$–$\epsilon$ and species equations. The boundary conditions for the fluid region are mass flow inlet, pressure outlet, symmetry and no-slip condition (at the interface with the solid domain).

The test case was modeled also with other near wall treatments, like the low-Reynolds $k$–$\epsilon$ turbulence model [35], and meshes with different refinement levels, but showed no significant differences respect the model described here.

### 3.3. Transpiring wall reactor

A model previously developed for describing the behavior of the transpiring wall reactor [23] was modified in order to describe the performance of the reactor with a hydrothermal flame inside, incorporating the kinetic model obtained in this work. The model assumes stationary conditions considering only mass and energy balances, resolved by the Runge–Kutta method of 4th order, while the momentum equation was neglected. The pressure along the reactor was considered constant and equal to 23 MPa. Enthalpy and heat capacities were calculated using PR-EoS. Densities were calculated by VTPR-EoS considering the exact composition of the mixture. Global heat transmission coefficients were calculated as a function of the total mass flow, and the coefficient for the heat transmission of the outer wall with the environment was taken as $0.5\,W\,m^{-2}\,K^{-1}$. The heat of reaction for IPA oxidation were calculated for different temperatures using a polynomial fit (Eq. (14)).

$$\Delta H_r(T) = \begin{cases} a_0 + a_1T + a_2T^2 + a_3T^3 + a_4T^4, & T \le 404\,^\circ C \\ b_0 + b_1T + b_2T^2 + b_3T^3 + b_4T^4, & T > 404\,^\circ C \end{cases} \tag{14}$$

where the coefficients of the polynomials are presented in Table 2.

This model assumes the injector as a PFR, the upper part of the reaction chamber as a CSTR, and the reaction chamber is modeled as a plug flow. The model includes heat exchange between injector and reaction chamber, and heat and mass exchange between reaction chamber and transpiring chamber. A complete description of the base model is given by Bermejo et al. [23].

**Table 2**
Coefficients of polynomial equation fitted for enthalpy of reaction of IPA oxidation as function of temperature at 23 MPa. Temperature in °C, enthalpy in J/mol.

| | | | |
|---|---|---|---|
| $a_0$ | $-2.0353 \times 10^6$ | $b_0$ | $-2.0780 \times 10^6$ |
| $a_1$ | $-5.7254 \times 10$ | $b_1$ | $9.7755 \times 10^2$ |
| $a_2$ | 4.5344 | $b_2$ | −1.7952 |
| $a_3$ | $-2.2537 \times 10^{-2}$ | $b_3$ | $1.4322 \times 10^{-3}$ |
| $a_4$ | $3.4218 \times 10^{-5}$ | $b_4$ | $-4.1826 \times 10^{-7}$ |

## 4. Results

### 4.1. Study of mixing influence

Fig. 2 shows the dispersion of species according the result of a non-reacting simulation of the tee-junction. Concentrations (in vertical axis) are normalized by the mass fraction of equilibrium, when the species are completely mixed. The simulation corresponds to an experiment using a feed flow of 5.9 kg/h with 4% mass isopropyl alcohol at 488 °C and 3.7 kg/h of air at 389 °C, both at 23 MPa, which gives a Reynolds number of 26,000.

For these conditions the simulation shows that IPA concentrations is stabilized nearly 10 cm after the mixing point. In our facility, the interval between two temperature measuring points was about 20 cm and the total length of the reactor was 1.5 m, making insignificant the mixing length. Thus, the hypothesis of instantaneous mixing is acceptable and the reactor can be modeled as plug flow. Also, a visual reference of the mixing process can be seen on detail in Fig. 2, where the simulated contours of IPA concentration are presented.

### 4.2. Kinetic model

The fitted parameters and their confidence interval (CI) are presented in Eq. (15). The confidence interval of the parameters was calculated by the Matlab function `nlparci` which calculates the 95% confidence intervals for parameters in nonlinear regression.

$$X = \begin{pmatrix} X_1 \\ X_2 \end{pmatrix} = \begin{pmatrix} 18.34896 \\ 12.65636 \end{pmatrix}, \qquad \mathrm{CI} = \begin{pmatrix} 17.9204 & 18.7775 \\ 12.3087 & 13.0040 \end{pmatrix} \tag{15}$$

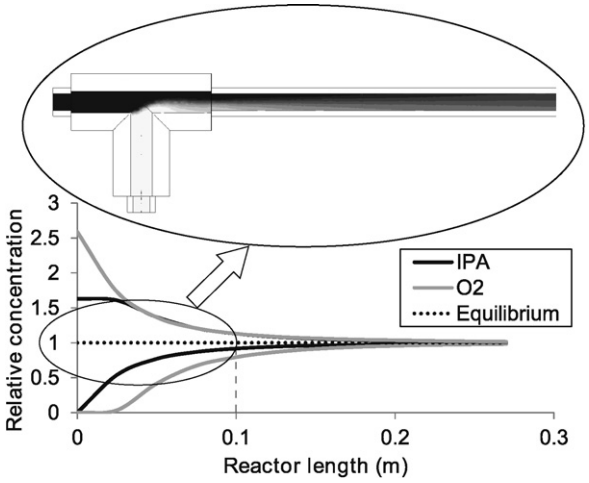


**Fig. 2.** Maximum and minimum species concentration relative to equilibrium concentration in the tubular reactor, showing the dispersion along reactor length: IPA (black line), $O_2$ (grey line). The central dotted line marks the equilibrium value. Above, detail of simulation: IPA (black), $O_2$ (white).

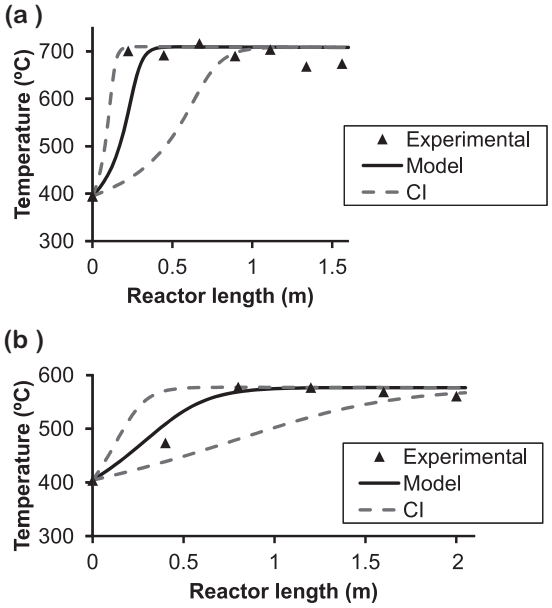


**Fig. 3.** Comparison of experimental temperatures (symbols) along the tubular reactor and model predictions (continuous line) using the fitted kinetics. Dashed lines indicate the predictions in the limits of CI. (a) 5.9 kg/h, 4%IPA at 395 °C, air as oxidant; (b) 10.6 kg/h, 2%IPA at 404 °C, $O_2$ as oxidant.

Thus, the kinetic parameters are shown in Eq. (16):

$$k_0 = (9.308 \pm 3.989) \times 10^7 (\mathrm{m^3\,s^{-1}\,kmol^{-1}})$$
$$E_a = 89.441 \pm 2.457 (\mathrm{kJ\,mol^{-1}}) \quad (16)$$

Fig. 3 compares the experimental temperature profile with the prediction of the model using the parameters found in Eq. (16). The data corresponds to experiments at two different inlet temperatures, flows and type of oxidant used: air or oxygen.

The model prediction agrees with experimental data, as the experimental temperatures are inside the model's interval of confidence. The least square error over all experimental points used to perform the fitting is 10.8%.

### 4.3. Parametric analysis

The kinetic model was applied in a parametric analysis to study the influence of inlet temperature and fuel concentration on flame formation. Once again, a plug flow reactor was assumed and the results are showed as function of residence time.

Fig. 4 shows how the fuel concentration affects the flame formation. Three different concentrations where tested at inlet temperature of 350 °C, and air in 10% excess. The analysis of the reaction rate shown in Fig. 4(a) indicates that a feed with 3% IPA at 350 °C is slowly oxidized, while a feed with 5% IPA is rapidly oxidized inside a narrow zone that could be recognized as a flame. Fig. 4(b) shows the temperature rising for the same cases and suggests a flameless oxidation for 3% IPA and a flame oxidation for 5% IPA. The concentration profiles are shown in Fig. 4(c) where can be seen a clear separation of reagents and products for the 5% IPA feed. These results are in accordance with the work of Serikawa [21], that found stable hydrothermal flames using a tubular reactor for IPA oxidation, when IPA concentrations were above 4% (or 5 vol%, since volume fraction was used in that work instead of mass fraction).

The effects of inlet temperature are shown in Fig. 5. Feeds with 5% IPA and air with 10% excess at three different injection temperatures are compared. Fig. 5(a) shows that the injection temperatures

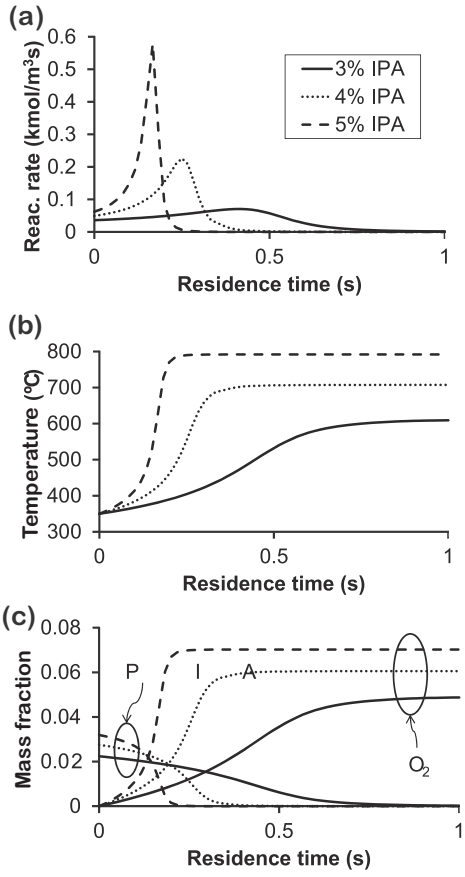


**Fig. 4.** (a) Reaction rate, (b) temperature and (c) species mass fractions as function of residence time in plug flow reactor at injection temperature of 350 °C for different inlet IPA concentrations: 3% (continuous line)), 4% (dotted line) and 5% (dashed line).

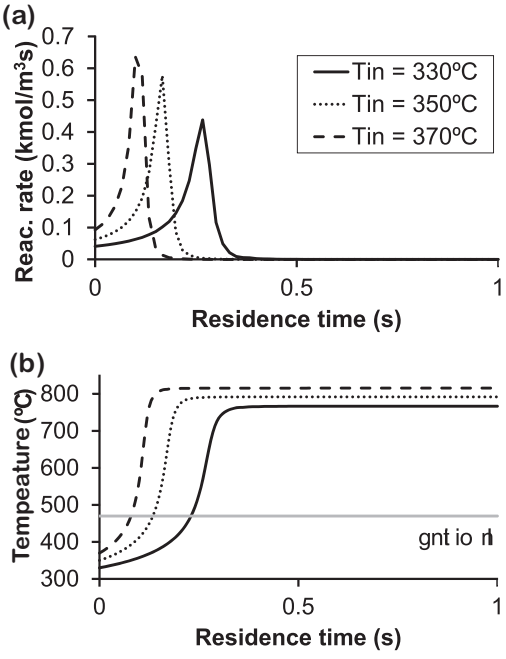


**Fig. 5.** (a) Reaction rate, (b) temperature as function of residence time in plug flow reactor at 5% IPA for different temperatures of injection: 330 °C (continuous line)), 350 °C (dotted line) and 370 °C (dashed line). Grey line corresponds to ignition temperature.

have influence on flame position. Reducing injection temperature from 370 to 330 °C causes a delay of approximately 0.2 s in the flame ignition. With the characteristics of our experimental plant, this delay is equivalent to a displacement of 60 cm. Fig. 5(b) shows temperature profiles for the three cases and the ignition temperature found by Serikawa [21]. This temperature (470 °C) corresponds to the beginning of the maximum slope region at temperature profiles predicted in this work.

### 4.4. Simulation of TWR

The result of the transpiring wall reactor simulation shown here corresponds to a piece of experimental data using a feed flow of 27.7 kg/h with 8% mass isopropyl alcohol and 23.9 kg/h of air, an injection temperature of 246 °C and a pressure of 23 MPa. The transpiring flow was 16.9 kg/h of water at 25 °C.

The results of this simulation show that the model correctly predicts the heating and flameless oxidation inside the injector and also the flame formation at upper part of reaction chamber. In presence of a hydrothermal flame, complete oxidation occurs when injection temperatures are as low as 246 °C. Inside the injector, the reagent stream is heated up to 382 °C due heat transmission from the reactor chamber through the injector's wall, and slow oxidation. Outside the injector, the reactive mixture reaches a temperature as high as 709 °C (experimental value was 694 °C). The temperature profile predicted by the model is compared to the experimental temperature data measured inside the injector and at the reaction chamber in Fig. 6(a). A good agreement with the experimental data can be observed here.

Fig. 6(b) shows the same experiment reproduced by the previous model of our group [23]. The kinetic model adopted in that previous work was able to reproduce experimental data for inlet temperatures of 300 °C and above, but failed at lower injection temperatures. Other models existing in literature, fitted for systems at lower temperatures, are not fast enough to correctly predict the rapid reaction rate at flame zone. Nevertheless, the model developed in this work shows satisfactory results for a wide range of inlet temperatures and concentrations.

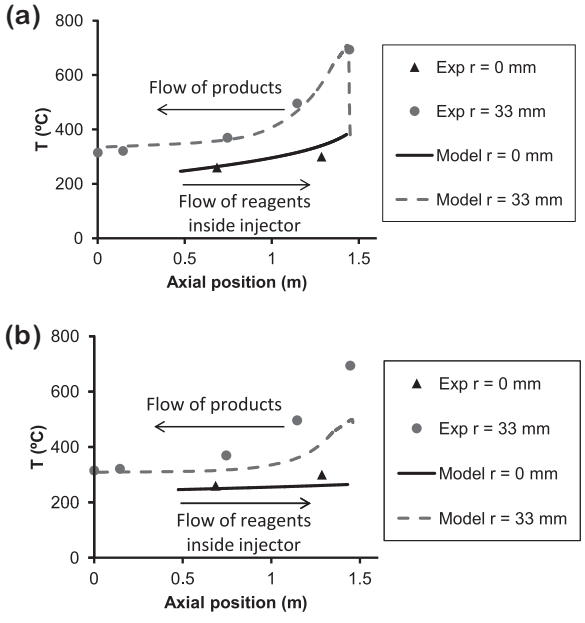


**Fig. 6.** Experimental (symbols) and model (lines) temperature profiles of TWR simulation: (a) this work, (b) previous model. Black color corresponds to injector; grey color represents reaction chamber.

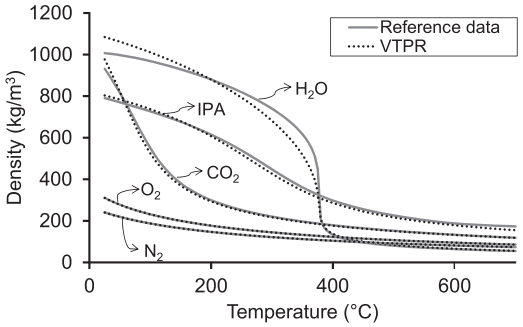


**Fig. A.7.** Density fitting for pure species using PR-EoS at 230 bar.

## 5. Conclusions

A new simple kinetic model for supercritical water oxidation of isopropyl-alcohol in hydrothermal flame regime was determined by adjusting the temperature profile in tubular SCWO reactors. The model is able to predict temperature profiles in tubular reactors at different IPA concentrations, feed flows and using air or oxygen as the oxidant.

A 3D CFD model confirmed the hypothesis that the mixing process occurs in the first centimeters of the tubular reactor. Thus, the initiation of the reaction is not affected by the mixing process, being the reaction controlled by the kinetics.

Given the inlet conditions, the model can estimate if the oxidation will be flame or flameless regime, and is capable of reproducing both.

This kinetic model was applied to a model for the transpiring wall reactor developed by the University of Valladolid and the experimental data were successfully described. According to the results, in the presence of a hydrothermal flame, the reactor can be maintained in steady state regime, with total destruction of fuel, even for subcritical feed injections (246 °C).

The new kinetic model, allied with modeling and simulation, allows for a better understanding of SCWO reactors and can lead to improving their design and optimization.

## Acknowledgments

The authors thank the Spanish Ministry of Science and Innovation for the CTQ2010-15475 Project (subprogram PPQ). J.P.S. Queiroz thanks the Spanish Ministry of Education's FPU program (AP2009-0399) for his PhD grant.

## Appendix A. Volume translation fitting

Fig. A.7 shows the fitting of the densities of pure compounds by VTPR-EoS. The continuous line corresponds to NIST data as a function of temperature at 230 bar, and the dotted line corresponds to the predicted densities. The volume correction was estimated for each substance in order to minimize the differences between the reference data and the predicted values. For isopropyl-alcohol, density data are not available on the NIST database, so the reference data were obtained by SR-Polar-EoS calculations in Aspen Plus.

## References

[1] M. Bermejo, M. Cocero, Supercritical water oxidation: a technical review, AIChE Journal 52 (2006) 3933–3951.
[2] G. Brunner, Near and supercritical water. Part II: oxidative processes, Journal of Supercritical Fluids 47 (2009) 382–390.
[3] C. Augustine, J. Tester, Hydrothermal flames: from phenomenological experimental demonstrations to quantitative understanding, Journal of Supercritical Fluids 47 (2009) 415–430.

[4] W. Schilling, E. Franck, Combustion and diffusion flames at high-pressures to 2000 bar, Berichte Der Bunsen-Gesellschaft-Physical Chemistry Chemical Physics 92 (1988) 631–636.
[5] C. Oh, R. Kochan, T. Charlton, A. Bourhis, Thermal-hydraulic modeling of supercritical water oxidation of ethanol, Energy & Fuels 10 (1996) 326–332.
[6] B. Wellig, M. Weber, K. Lieball, K. Prikopsky, P. von Rohr, Hydrothermal methanol diffusion flame as internal heat source in a SCWO reactor, Journal of Supercritical Fluids 49 (2009) 59–70.
[7] B. Wellig, K. Lieball, P. von Rohr, Operating characteristics of a transpiring-wall SCWO reactor with a hydrothermal flame as internal heat source, Journal of Supercritical Fluids 34 (2005) 35–50.
[8] M. Bermejo, P. Cabeza, M. Bahr, R. Fernandez, V. Rios, C. Jimenez, M. Cocero, Experimental study of hydrothermal flames initiation using different static mixer configurations, Journal of Supercritical Fluids 50 (2009) 240–249.
[9] M. Bermejo, C. Jimenez, P. Cabeza, A. Matias-Gago, M. Cocero, Experimental study of hydrothermal flames formation using a tubular injector in a refrigerated reaction chamber. Influence of the operational and geometrical parameters, Journal of Supercritical Fluids 59 (2011) 140–148.
[10] M. Bermejo, P. Cabeza, J. Queiroz, C. Jimenez, M. Cocero, Analysis of the scale up of a transpiring wall reactor with a hydrothermal flame as a heat source for the supercritical water oxidation, Journal of Supercritical Fluids 56 (2011) 21–32.
[11] C. Narayanan, C. Frouzakis, K. Boulouchos, K. Prkopsk, B. Wellig, P. Rudolf von Rohr, Numerical modelling of a supercritical water oxidation reactor containing a hydrothermal flame, Journal of Supercritical Fluids 46 (2008) 149–155.
[12] F. Vogel, J. Blanchard, P. Marrone, S. Rice, P. Webley, W. Peters, K. Smith, J. Tester, Critical review of kinetic data for the oxidation of methanol in supercritical water, Journal of Supercritical Fluids 34 (2005) 249–286.
[13] R.K. Helling, J.W. Tester, Oxidation of simple compounds and mixtures in supercritical water: carbon monoxide, ammonia and ethanol, Environmental Science & Technology 22 (1988) 1319–1324.
[14] L. Li, P. Chen, E. Gloyna, Kinetic-model for wet oxidation of organic-compounds in subcritical and supercritical water, Supercritical Fluid Engineering Science - Fundamentals and Applications 514 (1993) 305–313.
[15] J. Ploeger, P. Bielenberg, J. Dinaro-Blanchard, R. Lachance, J. Taylor, W. Green, J. Tester, Modeling oxidation and hydrolysis reactions in supercritical water-free radical elementary reaction networks and their applications, Combustion Science and Technology 178 (2006) 363–398.
[16] P. Webley, J. Tester, H. Holgate, Oxidation-kinetics of ammonia and ammonia–methanol mixtures in supercritical water in the temperature-range 530-degrees-c 700-degrees-c at 246 bar, Industrial & Engineering Chemistry Research 30 (1991) 1745–1754.
[17] T. Hunter, S. Rice, R. Hanush, Raman spectroscopic measurement of oxidation in supercritical water. 2. Conversion of isopropyl alcohol to acetone, Industrial & Engineering Chemistry Research 35 (1996) 3984–3990.
[18] S.P. Maharrey, D.R. Miller, A direct sampling mass spectrometer investigation of oxidation mechanisms for acetic acid in supercritical water, The Journal of Physical Chemistry A 105 (2001) 5860–5867.
[19] S. Rice, T. Hunter, A. Ryden, R. Hanush, Raman spectroscopic measurement of oxidation in supercritical water. 1. Conversion of methanol to formaldehyde, Industrial & Engineering Chemistry Research 35 (1996) 2161–2171.
[20] J. Sierra-Pallares, M. Parra-Santos, J. Garcia-Serna, F. Castro, M. Cocero, Numerical analysis of high-pressure fluid jets: application to RTD prediction in supercritical reactors, Journal of Supercritical Fluids 49 (2009) 249–255.
[21] R. Serikawa, Hydrothermal flames in supercritical water oxidation: investigation in a pilot scale continuous reactor, Fuel 81 (2002) 1147–1159.
[22] P. Cabeza, M. Bermejo, C. Jimenez, M. Cocero, Experimental study of the supercritical water oxidation of recalcitrant compounds under hydrothermal flames using tubular reactors, Water Research 45 (2011) 2485–2495.
[23] M. Bermejo, F. Fernandez-Polanco, M. Cocero, Modeling of a transpiring wall reactor for the supercritical water oxidation using simple flow patterns: comparison to experimental results, Industrial & Engineering Chemistry Research 44 (2005) 3835–3845.
[24] D.-Y. Peng, D.B. Robinson, A new two-constant equation of state, Industrial & Engineering Chemistry Fundamentals 15 (1976) 59–64.
[25] A. Peneloux, E. Rauzy, R. Freze, A consistent correction for Redlich–Kwong–Soave volumes, Fluid Phase Equilibria 8 (1982) 7–23.
[26] E.W. Lemmon, M.O. McLinden, D.G. Friend, Thermophysical properties of fluid systems, in: P.J. Linstrom, W.G. Mallard (Eds.), NIST Chemistry WebBook, NIST Standard Reference Database, 69, National Institute of Standards and Technology, Gaithersburg, MD, 2011, Last access: 06/30/2012.
[27] J. Schwartzentruber, H. Renon, S. Watanasiri, Development of a new cubic equation of state for phase equilibrium calculations, Fluid Phase Equilibria 52 (1989) 127–134.
[28] K.S. Lieball, Numerical Investigations on a Transpiring Wall Reactor for Supercritical Water Oxidation, Doctor of Technical Sciences, Swiss Federal Institute of Technology Zurich, Zurich, 2003.
[29] L. Li, P. Chen, E. Gloyna, Generalized kinetic-model for wet oxidation of organic-compounds, AIChE Journal 37 (1991) 1687–1697.
[30] K. Levenberg, A method for the solution of certain problems in least squares, The Quarterly of Applied Mathematics 2 (1944) 164–168.
[31] D. Marquardt, An algorithm for least-squares estimation of nonlinear parameters, SIAM Journal on Applied Mathematics 11 (1963) 431–441.
[33] ANSYS, ANSYS FLUENT 12.0 Theory Guide, 2009.
[33] B.E. Poling, J.M. Prausnitz, J.P. O'Connell, The Properties of Gases and Liquids, 5th ed., McGraw-Hill, New York, 2007.
[34] J. Sierra-Pallares, M. Parra-Santos, J. Garcia-Serna, F. Castro, M. Cocero, Numerical modelling of hydrothermal flames. Micromixing effects over turbulent reaction rates, Journal of Supercritical Fluids 50 (2009) 146–154.
[35] B.E. Launder, B.I. Sharma, Application of the energy-dissipation model of turbulence to the calculation of flow near a spinning disc, Letters in Heat and Mass Transfer 1 (1974) 131–138.